

# COMPARISON OF FULL 3D-RANS SIMULATIONS WITH 2D-RANS / LIFTING LINE METHOD CALCULATIONS FOR THE FLOW ANALYSIS OF RIGID WINGS FOR HIGH PERFORMANCE MULTIHULLS

**K. Graf**, Yacht Research Unit - Univ. Applied Sciences Kiel, Germany, kai.graf@fh-kiel.de

**A. v. Hoeve**, Technical University Delft, The Netherlands, advanhoeve@gmail.com

**Simon Watin**, VPLP Yacht Design, Vannes / France, watin@vannes.vplp.fr

**Abstract:** This paper reports about a comparison of a 3D RANS investigation to calculate the flow around wing sails with a method based on 2D RANS calculations of flow around wing profiles in conjunction with a lifting line method to account for 3-dimensional flow phenomena. The investigation focusses on rigid wings with two elements: a main element with a hinged flap, as they are currently used on some performance multihulls. Wing sails can be analyzed using conventional 3D RANS flow investigation methods; however the computational costs are quite high. Here an alternative approach is introduced. It is based on planar flow 2D RANS profile investigations in conjunction with a lifting line method to account for 3-dimensional flow phenomena and induced drag. The lifting line method uses an iterative approach to make use of non-linear profile lift coefficients. This approach is so computational efficient that it can be combined with constrained optimization methods in order to optimize performance of the wing. The paper describes the motivation for the development, the lifting line theory and validation efforts. Some applications of the new method are shown, demonstrating the ability of the method to be used for wing sail design and operation optimization.

**Key words:** wing sails; lift; induced drag; RANS; Lifting line method; America's Cup

## NOMENCLATURE

$AoA$	Angle of Attack (-)
$AWS$	Apparent wind speed (m/s)
$AWA$	Apparent wind angle (rad if not defined otherwise)
$\beta$ , $\beta_{flap}$	Flap angle (rad if not defined otherwise)
$c$	Profile Length (m)
$c_D$	Drag coefficient (-)
$c_L$	Lift coefficient (-)
$D_i$	Induced drag
$L$	Lift (N)
$L$	$ L $ (N)
$\mathbf{r}$	Vector from point to integrator $ds$ (m)
$r$	$ \mathbf{r} $ (m)
$\mathbf{s}$	vector along filament (m)
$s_{eff}$	Effective span (m)
$\mathbf{u}$	Flow Velocity vector (m/s)
$v$	Induced wind speed (m/s)
$w_{FVF}$	Lower free vortex filament weighting (-)
$x$	Longitudinal coordinate (m)
$y^+$	Dimensionless wall distance (-)
$z$	Vertical span-wise coordinate (m)
$z_{fvf}$	Vertical coordinate of free vortex filament (m)
$z_C$	Vertical coordinate of the panel center (m)
$z_1, z_2$	Coordinates of lower and upper bound of wake sheet (m)
$\lambda$	Aspect ratio of wing (-)
$\Gamma$	Vorticity (m <sup>2</sup> /s)
$\Delta\Gamma_{bound}$	Stepwise change of bound vorticity (m <sup>2</sup> /s)
$\Gamma_{bound}$	Vorticity of bound vortex filament (m <sup>2</sup> /s)
$\Gamma_{fvf}$	Vorticity of free vortex filament (m <sup>2</sup> /s)
$\Gamma_1, \Gamma_2$	Vorticity at lower and upper bounds of wake sheet (m <sup>2</sup> /s)
$\rho$	Density (kg/m <sup>3</sup> )
$\omega$	Relaxation factor (-)
SI units only	

## 1 INTRODUCTION

Multihulls are getting increasingly popular in contemporary sail sport. Modern lightweight sports catamarans or trimarans achieve high boat speed under sail and thus provide extraordinary sailing fun. Sport multihulls easily achieve boat speeds higher than wind speed. Consequently the apparent wind angle – the angle between the yacht's centerline and the incident wind – is rather small. Even on downwind courses, the apparent wind angle commonly is smaller than  $90^\circ$ . Under these circumstances the performance of a wind propulsion system is dominated by its lift to drag ratio. Compared to conventional soft sails, rigid wing sails, similar to airplane wings, provide higher lift to drag ratios, in many cases more than twice the value. This makes them particularly suitable to be used on high speed sailing multihulls. Wing sails became popular with the *Little America's Cup*, an international sailboat race on approximately 6 m long catamarans. Here rigid wing sails are used since more than 30 years.

With the decision to sail the races of the 34<sup>th</sup> *America's Cup* on catamarans of type AC72 featuring multi-element rigid wings, wing sails came into the focus of designers, engineers and scientists involved in the design of the respective yachts. The *America's Cup*, a professional sail sport event well known for its high level of science and engineering applied to the development of the yachts, has boosted the demand in accurate and efficient flow analysis methods applicable to wing performance prediction. Figure 1-1 shows the winner of the 34<sup>th</sup> America's Cup, the yacht of *Oracle Team USA*.



Figure 1-1: Oracle Team USA in the 2013 America's Cup  
Foto: Donan.Raven, License: CreativeCommons by-sa-3.0-de

Typical analysis methods for the three-dimensional flow around such wings are 3D-RANS flow simulations. They are well-suited for rigid wings, since they are able to take into account the viscous and turbulent flow phenomena that are crucial for the operation of these wings with small gaps between the elements. However an assessment of the performance of a wing requires the execution of a quite complex test matrix, being defined by the permutation of angles of attack, twist and flap angles to be investigated. With a single RANS simulation using finite volume discretization of about 10 to 30 million grid cells, the computational burden for the execution of a full test matrix for single wing geometry is very large.

A remedy to this problem are flow analysis methods based on the combination of a lifting line method in conjunction with profile lift and drag data generated from 2D-RANS simulations. 2D-RANS simulations are dramatically less

computational expensive than 3D-RANS simulations and can predict the complex flow pattern around a multi-element profile with gaps while lifting line methods take care of three dimensional flow phenomena, in particular induced drag. This method promises to be far less computational demanding than 3D-RANS investigations.

A rough estimate of the amount of computations necessary for a full wing analysis quantifies the motivation behind the present work: for an assessment of the performance of a wing (for example by a velocity prediction program) a permutation of angles of attack, flap angles and twist has to be investigated. A small test matrix for a single multi-element-wing geometry (neglecting Reynolds number changes) would consist of about 10 angles of attack, each combined with 2 to 4 base flap angles and 2 to 4 twist angles to cover a minimum range of operational states covering non-linear effects due to separation. A 3D-RANS investigation would thus consist of more than 100 computational simulations of a grid of about 10 to 30 million grid cells as a minimum. In contrast to this a profile investigation will investigate a two to four 2-element profile shapes in order to account for profile variations with span, each shape investigated with a computational grid of about 50000 to 300000 grid cells. Each profile will be investigated at about 10 angles of attack and 2 to 4 flap angles. The effect of twist will be taken into account by the lifting line approach. Since the computational costs of the lifting line method itself is negligible compared to the computational load of even the smallest RANS investigation, the 2D-RANS – lifting line approach theoretically reduces the computational burden for the investigation of a wing by the factor of 100. Even more, a variation of the planform of the wing would require redoing almost the entire test matrix of the 3D-RANS investigations, while in a first approximation no need for additional 2D-RANS simulation exists for the 2D-RANS – lifting line method as long as the thickness ratio and the relative chord length of main and second element profiles remain constant. Consequently the computational burden for the investigation of for example 10 wing planforms for a variational study of planform can be reduced by the factor of 1000.

Obviously the accuracy of the 2D-RANS – lifting line method has to be proven and has to provide the same level of confidence as the 3D-RANS method. The description of the 2D-RANS – lifting line method and the comparison with 3D-RANS results are the main foci of this paper. In addition some practical applications are shown, making use of the computational efficiency of the new method.

This paper focusses on rigid wings and profiles of two elements: the symmetric main element which is assumed to be completely rigid and a hinged flap, which can be rotated around an axis, lying somewhere on the center line of the main element. The flap is divided in span-wise direction into a couple of panels, allowing changing the flap angle with height in order to twist the wing. Obviously the entire wing can be rotated around a vertical axis resting on a wing step on the catamaran platform. Sailing yachts usually encounter a twisted incident wind, e.g. the apparent wind angle and the apparent wind speed change with height above water plane. While 3D-RANS investigations model this using appropriate boundary conditions, the approach based on 2D-RANS investigations and a lifting line method take this into account by using an effective incident wind depending on the height of the profile above water plane.

## 2 THE LIFTING LINE METHOD

The lifting line method is based on the following principal: a bound vortex filament of piecewise linear, optionally discontinuous, vorticity distribution along span is running from root to tip of the wing. Individual free vortex filaments and/or wake sheets (in any combination) are shedding from bound vortex filaments into infinity in the direction of incident flow. Discrete vorticities of the free vortex filaments and the distributed vorticity per length of the wake sheet are calculated conforming to *Thompsons* rule: (i) a linear change of vorticity of the bound filament generates a wake sheet of constant vorticity per span length and (ii) a discontinuity of vorticity of the bound vortex filament generates a discrete free vortex filament, its vorticity being the jump of vorticity of the bound filament at the location of the discontinuity. Induced wind is calculated from the free vortex filaments and the wake sheet using *Biot Savart's* law. The vector sum of induced wind and undisturbed incident flow gives an effective incident flow. The lift – calculated from *Kutta's* law – acts perpendicular to it. This effective lift can be decomposed into a flow force perpendicular to the undisturbed incident flow – the nominal lift – and an additional flow force in the direction of the undisturbed flow – the induced drag. The discrete form of this method calculates the total drag as integration over span of the induced drag per span plus the viscous profile drag. In a similar manner the profile lift is integrated over span, taking into account the local effective incident flow.

The standard inversed lifting line method assumes linear variation of the lift coefficient with angle of attack, see Truelsen and Schlichting (1967). It involves the inversion of a matrix in order to calculate the discrete spanwise vorticity distribution of the bound vortex filament for a given geometry. However to take into account nonlinear lift coefficients with respect to angle of attack, in particular lift coefficient changes due to flow separation, an iterative approach is employed here. It is based on an iterative correction of induced wind from the spanwise lift distribution which takes into account the induced wind as a correction of angle of attack. The approach implemented here is similar to the method described by Anderson (2011). Anderson uses a continuous vortex distribution along the lifting line,

integrating it using Simpson numerical integration, while the method employed here uses continuous, stepwise linear vorticity distribution as well as a discontinuous change of the vorticity in any arbitrary combination. The rationale behind this approach was to better model the vorticity distribution close to the tip of a wing with a non-zero chord length at the tip.

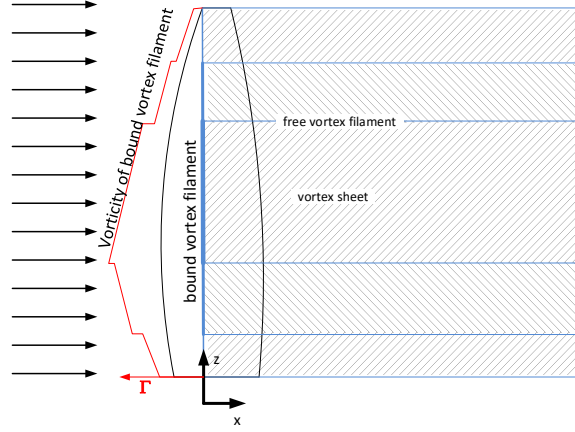


Figure 2-1: Bound and free vortex filaments on a wing

## 2.1 THEORY

Theorems of *Kutta*, *Biot-Savart* and *Thompson* are used as follows:

*Kutta's Law* is used to calculate the lift generated by a vortex filament:

$$\mathbf{L} = \int_{span} \rho \mathbf{u} \Gamma \times d\mathbf{s} \quad (2-1)$$

where  $\mathbf{L}$  is the generated lift,  $\rho$  the density of flow,  $\mathbf{u}$  the incident flow,  $\Gamma$  the vorticity of filament and  $d\mathbf{s}$  an integrator along the filament.

*Biot-Savart's Law* is used to calculate the induced wind generated by a free vortex filament:

$$\mathbf{v} = \frac{-1}{4\pi} \int_s \Gamma \frac{\mathbf{r} \times d\mathbf{s}}{|\mathbf{r}|^3} \quad (2-2)$$

where  $\mathbf{v}$  is the induced velocity generated by the vortex filament of vorticity  $\Gamma$  and  $\mathbf{r}$  is a vector from the point, where  $\mathbf{v}$  is generated to the integrator  $d\mathbf{s}$  along the filament.

Free vortex filaments are calculated by *Thompsons* rule, saying that a vortex filament may only end at a fixed wall or at infinity. *Prandl's* concept of horseshoe vortices is used, saying that any change of the bound vortex filament results in a free vortex filament. This results in:

$$d\Gamma_{fvf} = \frac{\partial \Gamma_{bound}(z)}{\partial z} dz \quad (2-3)$$

For a stepwise change of the vorticity of the bound vortex filament  $\Delta\Gamma_{bound}$ , the vorticity of the free vortex filament at the position of the stepwise change calculates from:

$$\Gamma_{fvf} = \Delta\Gamma_{bound} \quad (2-4)$$

A free vortex filament of constant vorticity  $\Gamma_{fvf}$  (from a stepwise change of  $\Gamma_{bound}$  as to (2-4)) starting at  $x=0$ ,  $z=z_{fvf}$ , running at constant  $z$  to  $x=\infty$ , generates induced wind in  $\mathbf{P}$  by (see Figure 2-2):

$$\begin{aligned}
v &= \frac{-\Gamma_{fif}}{4\pi} (z_{fif} - z_C) \int_{x=0}^{\infty} \frac{dx}{r^3} \\
&= \frac{-\Gamma_{fif}}{4\pi} (z_{fif} - z_C) \left( \frac{x}{(z_{fif} - z_C)^2 r} \right) \Big|_{x=0}^{\infty}
\end{aligned} \tag{2-5}$$

This yields (with  $x/r = 1$  for  $x \rightarrow \infty$ ):

$$v = \frac{-\Gamma_{fif}}{4\pi} \frac{1}{z_{fif} - z_C} \tag{2-6}$$

A vortex filament sheet generated from a span-wise change of  $\Gamma_{bound}(z)$  starting at  $z_1$  till  $z_2$  induces wind according to (see Figure 2-2):

$$v = \frac{-1}{4\pi} \int_{z_1}^{z_2} \frac{\partial \Gamma_{bound}}{\partial z} \frac{dz}{z - z_C} \tag{2-7}$$

We assume  $\Gamma_{bound}$  changes linear between  $z_1$  and  $z_2$  from  $\Gamma_1$  to  $\Gamma_2$ :

$$\Gamma_{bound}(z) = \Gamma_1 + \frac{\Gamma_2 - \Gamma_1}{z_2 - z_1} (z - z_1) \tag{2-8}$$

Introducing the constant expression:  $\partial \Gamma_{bound} / \partial z = (\Gamma_2 - \Gamma_1) / (z_2 - z_1)$  into (2-7) yields:

$$\begin{aligned}
v &= \frac{-1}{4\pi} \frac{\Gamma_2 - \Gamma_1}{z_2 - z_1} \int_{z_1}^{z_2} \frac{dz}{z - z_C} \\
&= \frac{-1}{4\pi} \frac{\Gamma_2 - \Gamma_1}{z_2 - z_1} \ln \left( \frac{z_2 - z_C}{z_1 - z_C} \right)
\end{aligned} \tag{2-9}$$

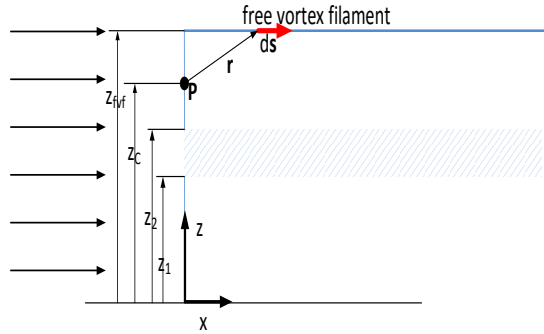


Figure 2-2: Free vortex filament and wake sheet generating lift at arbitrary point **P**

Profile lift per span length  $L=d|L|/dz$  is calculated from a lift coefficient  $c_L$ , the dynamic pressure  $0.5\rho u^2$  (density  $\rho$ , flow speed  $u=|\mathbf{u}|$ ) and the profile chord length  $c$ .  $c_L$  depends nonlinear on angle of attack  $AoA$  of incident flow. For a profile of a wing of finite span the angle of attack is  $AoA$  reduced by induced wind:

$$L = 0.5 \rho A W S^2 c \quad c_L (AoA - v / AWS) \tag{2-10}$$

The induced drag then calculates from

$$D_i = L v / AWS \tag{2-11}$$

The bound vorticity of the profile is calculated from the lift per span length due to (2-1)

$$\Gamma_{bound} = \frac{L}{\rho AWS} \quad (2-12)$$

Since vorticity of free vortex filament depends on vorticity of bound vortex filament, which in turn depends on lift, itself depending on free vortex filament vorticity due to induced wind, this procedure is iterative by nature.

For a wing of finite span with varying lift distribution over span the iterative procedure is:

- (1) Assume  $v=0$
- (2) Calculate profile lift per span from (2-10) for a given geometric angle of attack, flow speed and chord length
- (3) Calculate  $\Gamma_{bound}$  over span from profile lift from (2-12)
- (4) Calculate  $v$  from (2-6) and (2-9)
- (5) redo 2.-5. until  $v$  converges
- (6) calculate induced drag
- (7) calculate total drag by adding parasitic profile drag to induced drag

## 2.2 DISCRETIZATION

The envelope of the wing is discretized with an arbitrary number of horizontal profiles, numbered  $i=0,1,\dots,N$ . Each profile is described by its  $z$ -coordinate  $z_i$ , a chord length  $c_i$  along with leading and trailing edge  $x$ -coordinates, an individual incident flow speed  $AWS_i$ , an incident (geometric) angle of attack  $AoA_i$ , a lift coefficient  $c_{Li}$ , a parasitic profile drag coefficient  $C_{DPPi}$  and a moment coefficient  $C_{Mi}$  with respect to a local origin, for example the leading edge. No profile geometry is needed since the property of the profile is entirely described by the lift coefficient. However additional parameters can be used to change the flow force coefficients, for example the angle of a hinged flap of the profile. The planform area of the wing is defined by trapezoidal panels, number  $i=1,2,\dots,N$  between profiles  $i-1$  and  $i$ . Due to the definition by neighboring profiles, panels can have varying incident speed and angle of attack and can twist.

Flow force coefficients  $c_L$ ,  $C_{DPP}$  and  $C_M$  can be provided by tabulated data for given  $AoA$  and additional parameters like a flap angle  $\beta$ . This approach allows taking into account profile properties from any source, being it linear or nonlinear, from inviscid or viscous calculation methods.

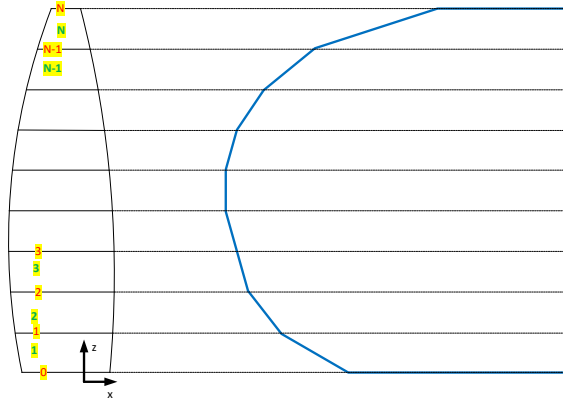


Figure 2-3: Discretization of wing planform

A bound vortex filament at  $x=0$  aligned with the  $z$ -axis for incident flow aligned with the  $x$ -axis is assumed. The vorticity  $\Gamma$  changes linear between profiles, generating a free vortex wake sheet. At bottom profile (root) and top profile (tip) discrete free vortex filaments are generated in order to satisfy zero bound vorticity for  $z < z_0$  and  $z > z_N$ . Consequently  $\Gamma_{bound}(z)$  and  $\Gamma_{jvf\ root}$  as well as  $\Gamma_{jvf\ tip}$  can be calculated from profile definition information:

for  $0 \leq i \leq N$ :

$$\Gamma_i = 0.5 AWS_i c_i c_{Li} (AoA_i - \frac{v_i}{AWS_i}) \quad (2-13)$$

for  $z_i < z < z_{i+1}$

$$\Gamma_{bound}(z) = \Gamma_i + \frac{\Gamma_{i+1} - \Gamma_i}{z_{i+1} - z_i} (z - z_i) \quad (2-14)$$

$$\Gamma_{fvf\ root} = -\Gamma_0 w_{FVF} \quad (2-15)$$

$$\Gamma_{fvf\ tip} = \Gamma_N \quad (2-16)$$

Here  $w_{FVF}$  is a factor taking into account to which degree the root free vortex filament is suppressed by a wall. If the root of the wing is fixed to a wall without a gap,  $w_{FVF}=0$ . If no wall is present at all,  $w_{FVF}=1$ .  $w_{fvf}$  can be calculated from a known result at a particular  $AoA$ .

Induced wind is calculated in the vertical center of each panel  $j=1,2,\dots,N$  by summing up the induced wind generated by any free vortex wake sheet and the discrete free vortex filaments at root and tip.

$$\begin{aligned} v_{Cj} = & \frac{-1}{4\pi} \sum_{i=1}^N \frac{\Gamma_i - \Gamma_{i-1}}{z_i - z_{i-1}} \ln\left(\frac{z_i - z_{Cj}}{z_{i-1} - z_{Cj}}\right) \\ \text{for } 1 \leq j \leq N: & \\ & + w_{FVF} \frac{\Gamma_0}{4\pi} \frac{1}{z_0 - z_{Cj}} + \frac{-\Gamma_N}{4\pi} \frac{1}{z_N - z_{Cj}} \end{aligned} \quad (2-17)$$

where  $z_{Cj} = 0.5(z_j + z_{j-1})$  is the  $z$ -coordinate of the panel center and  $v_{Cj}$  the induced wind at  $x=0$ ,  $z=z_{Cj}$ .

Linear interpolation is used to calculate induced wind  $v_i$  at profile vertical location  $z_i$ :

$$v_i = 0.5(v_{Ci+1} + v_{Ci}) \text{ for } 1 \leq i \leq N-1 \quad (2-18)$$

At root and tip induced wind is calculated using linear extrapolation:

$$v_0 = 2v_{C1} - v_1 \quad (2-19)$$

$$v_N = 2v_{CN-1} - v_{N-1} \quad (2-20)$$

An iterative procedure has to be used in order to calculate induced wind. We assume that for any profile  $i$ , the local height  $z_i$ , the profile length  $c_i$ , the local geometric angle of attack  $AoA_i$  and the local wind speed  $AWS_i$  is given. We also assume that lift coefficient can be calculated using the above values. Induced wind then is calculated iteratively starting with a zero guess:

- (1) Set  $v_i=0$  for any profile  $i=0,1,\dots,N$
- (2) Predict profile lift coefficient  $c_{Li}(AoA_i - v_i / AWS_i)$  using tabular data from 2D RANS profile solutions
- (3) Calculate  $\Gamma_i$  for any profile using (2-13)
- (4) Calculate induced wind in panel center  $v_{Ci}$  from (2-17)
- (5) Calculate induced wind at profile height from (2-18), (2-19) and (2-20)
- (6) Repeat (2) to (5) until convergence, if convergence achieved continue
- (7) Calculate lift per span for any profile using (2-10)
- (8) Calculate induced drag per span for any profile using (2-11) and add parasitic profile drag per span
- (9) calculate driving and side force per span from trigonometric relationship
- (10) Integrate over span by trapezoidal integration

It has to be taken into account, that direct integration of lift and drag over span is not feasible since their direction changes with height due to a twisted incident wind over wing span. Hence lift and drag is transformed to driving and side forces which allow integration over span independent of local incident wind.

To achieve convergence, the iterative procedure needs under-relaxation. If  $k$  denotes the current iteration step, the induced wind is calculated as a weighted average of the result of the current and last iteration step:

$$v_{Ci}^k = v_{Ci} \omega + v_{Ci}^{k-1} (1 - \omega) \quad (2-21)$$

where  $v_{Ci}$  is the induced wind as calculated from (2-17). Calculation of driving and side force is necessary if undisturbed incident wind angle of attack changes over height (wind twist). In this case no global lift and drag can be calculated. Some attention has to be paid to the angle of attack  $AoA$ , usually defined by the angle between incident wind and a reference line of the profile (for the profile of a symmetric main element this is its center line). The angle of incidence  $AoA$  is calculated from the apparent wind angle  $AWA$  and the local rotation of the profile, given by wing rotation and wing geometric twist with respect to the sailing yacht center line, which is the reference line of the apparent wind angle. This allows taking into account the sheeting of the wing, the twisting of the wing and a twist of the incident wind.

### 2.3 IMPLEMENTATION

The method is implemented as a spreadsheet calculation using MS Excel. The iterative method to predict induced wind is implemented as an embedded Visual Basic application. Under-relaxation factors around  $\omega = 0.25$  are used, which achieve convergence usually after 15 to 30 iteration cycles. The runtime on an average PC for a single prediction of flow forces of a two-element wing, discretized with 21 profiles, was about 1 to 3 sec.

## 3 RANS METHOD

The commercial RANS solver *StarCCM+* has been used for 2D- and 3D- flow simulations around profiles and wings. An introduction of RANS methods is not given here, for a general introduction refer to Ferziger and Perić (2008). An example of application of RANS methods to yacht flow investigations conducted by one of the authors is given in Böhm and Graf (2010).

The method used here is based on the solution of mass and momentum equations for incompressible adiabatically flow. For external flow at low Mach number the assumption of incompressible flow can be accepted. A finite volume discretization based on Cartesian hexahedral cells in the far field and body fitted prism cells in the vicinity of the flow body are used. Turbulence is taken into account using eddy viscosity hypothesis and the SST turbulence model for the prediction of turbulence viscosity. For some profile investigations however a Reynolds stress model has been used, see details below. For 3D-investigations, logarithmic wall functions were employed for the sake of computational efficiency. For 2D-profile investigations, some cases have been investigated employing wall functions, while other resolved the boundary layer.

All of the investigations shown here were executed on a Linux-based compute clusters. A maximum of 30 partitions/cores have been allocated to a particular 3D-run, while 2D-runs typically employed four to eight cores.

## 4 TEST CASES

Two test cases based on publicly available geometries are investigated:

- A rectangular foil of aspect ratio 4.5 with a 4-digit NACA profile
- A two-element wing in accordance with the AC72 class rules, however with some simplifications and approximations on main element and flap profile shape in order to reduce the computational load.

Both test cases have been investigated employing full 3D-RANS investigations and 2D-RANS profile investigations in combination with the lifting line method as described above. For the rectangular foil wind tunnel test results have been available for validation.

### 4.1 RECTANGULAR WING

The rectangular wing has a span of 1.8 m and a constant symmetric profile of type NACA 0012 with a profile chord length of 0.4 m. The root of the wing is fixed to a flat plate; see Figure 4-1, showing the wing together with the computational domain as well as the wing in the wind tunnel.

The wing as well as the profile are investigated at a Reynolds number of  $Rn = 1.28e5$ . The turbulence intensity at the inlet of the computational domain has been set to 1%, the value known from CTA field measurements in the wind tunnel. Since the simulations are carried out assuming fully turbulent flow, the wind tunnel model was equipped with turbulence stimulators, adhesive strip of 0.25\*5 mm cross section dimensions, see Figure 4-1.

A polyhedral grid of approximately 2.2 million grid cells is used for spatial discretization for the 3D test case, featuring a cascading refinement of the region around the wing and downstream of it, see Figure 4-2. Prism cells are used to resolve the boundary layer. Dimensionless wall distance of the cells contacting the wing is about  $20 < y^+ < 100$ .



The grid for the 2D-RANS investigation has been derived from the 3D-grid via a cut at the root of the wing. The respective 2D grid contains approximately 20000 grid cells, see Figure 4-3.

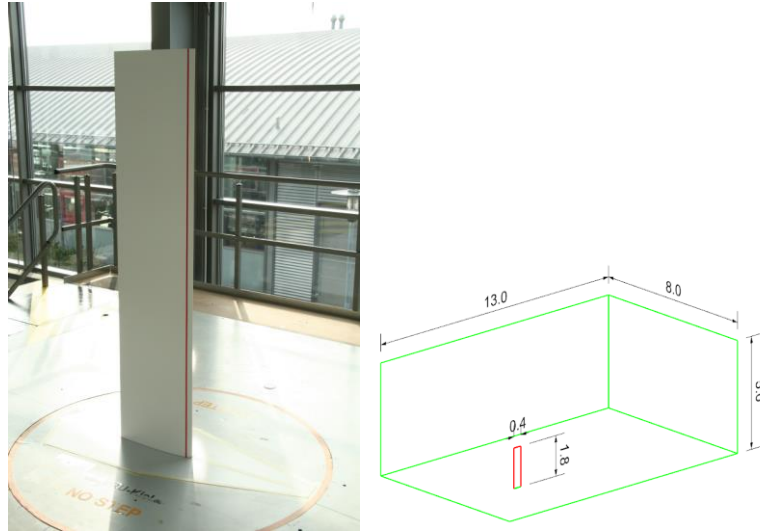


Figure 4-1: Rectangular wing and computational domain

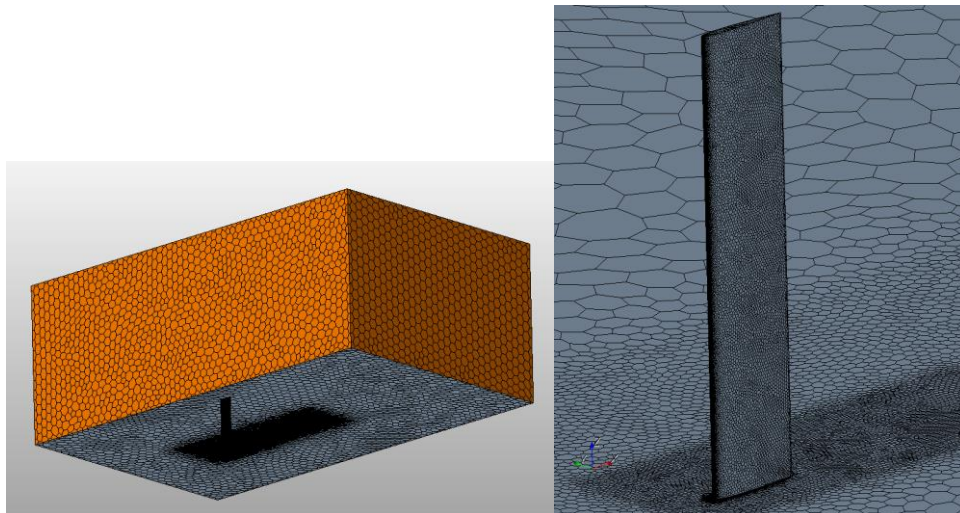


Figure 4-2: Polyhedral grid for 3D RANS investigation of rectangular grid

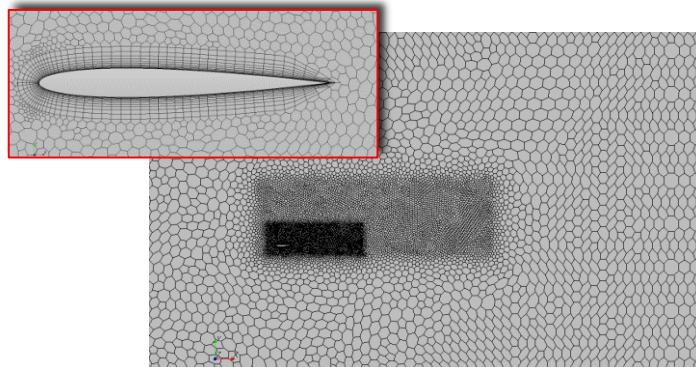


Figure 4-3: Computational grid around NACA 0012 profile for 2D-RANS simulation

Figure 4-4 shows lift and drag coefficients as the result of the 2D-RANS investigation. The diagram depicts the expected results for attached flow condition and beginning flow separation at an angle of attack of approximately  $10^\circ$ . At larger angles of attack the lift coefficient recovers and increases again. A similar pattern has been observed by Anderson (c2011), investigating a rectangular wing and comparing it with available wind tunnel results. However it is a well-known deficiency of common turbulence model that they inaccurately model flow separation. Hence the results for angles of attack  $AoA > 15^\circ$  must be viewed with caution.

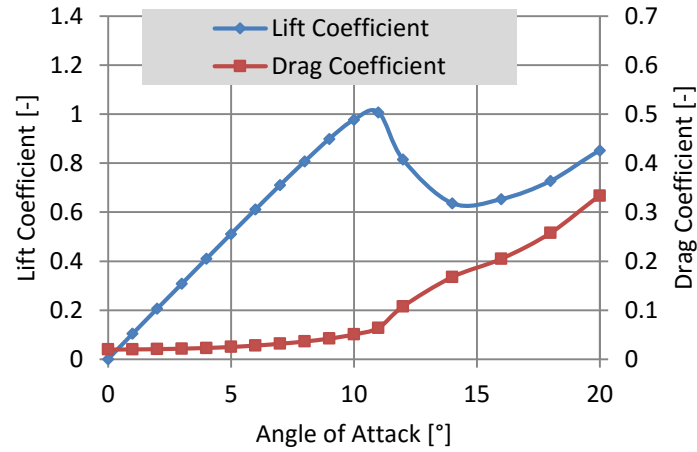


Figure 4-4: Lift and drag coefficients of the rectangular wing profile

The lifting line method uses 21 profiles, distributed evenly over span. The result of the 2D-RANS investigation is used to calculate lift and parasitic drag coefficients.

#### Comparison with 3D-RANS investigations and wind tunnel result:

Figure 4-5 shows lift and drag coefficients for 3D-RANS investigation in comparison with the result of the lifting line method and wind tunnel results. In addition estimated lift and drag coefficients from well-known and established formulas are plotted. The lift coefficient is calculated from Söding's formula, (Söding, 1982):

$$C_L = 2\pi AoA \frac{\lambda(\lambda+1)}{(\lambda+2)^2} \quad (4-1)$$

where  $\lambda = 2span / chordlength$  is the effective aspect ratio of the wing. The drag coefficient is calculated using:

$$C_D = C_L^2 \left( \frac{1}{\pi\lambda} + KPP \right) + 2(1+k) \frac{0.075}{(\log Rn - 2)^2} \quad (4-2)$$

where the frictional drag is calculated using the ITTC 57 friction line, see Harvald (1983),  $(1+k)=1.22$  is the form factor of the profile and  $KPP=0.02$  accounts for the parasitic profile drag.

The diagram shows fairly well agreement of 3D-RANS solution flow force coefficients with wind tunnel results at lower angles of attack. Lift coefficients are slightly over-predicted by the lifting line method. The angle of attack of maximum lift coefficient agrees well for all methods. It is slightly postponed to larger angles compared to the 2D-RANS results, this certainly the effect of the induced wind, which reduces the effective angle of attack. Maximum lift coefficient of wind tunnel test result is lower than the respective value from simulations and flow separation is less pronounced. This is observed frequently. Conventional RANS solvers predict flow separation differently than it is observed in experiments, this phenomenon depending on turbulence intensity and length scale in the wind tunnel. In particular the breakdown of lift with beginning separation is predicted differently. A possible explanation for this may be the length scale of turbulence in the wind tunnel. While the turbulence intensity in the wind tunnel is known from LDA measurements and thus can be taken into account by the simulation properly, the (largest) length scale of the turbulence in the wind tunnel is not known. Strong turbulence is known to have a blurring effect on the onset of separation. At higher angles of attack drag coefficients from the simulation are lower than those from wind tunnel tests. Again this may be assigned to a lack of existing turbulence models to properly resolve separated flow.

In general it can be observed that the agreement of 3D-RANS simulations with the method based on 2D-RANS simulations in combination with the lifting line method is rather good.

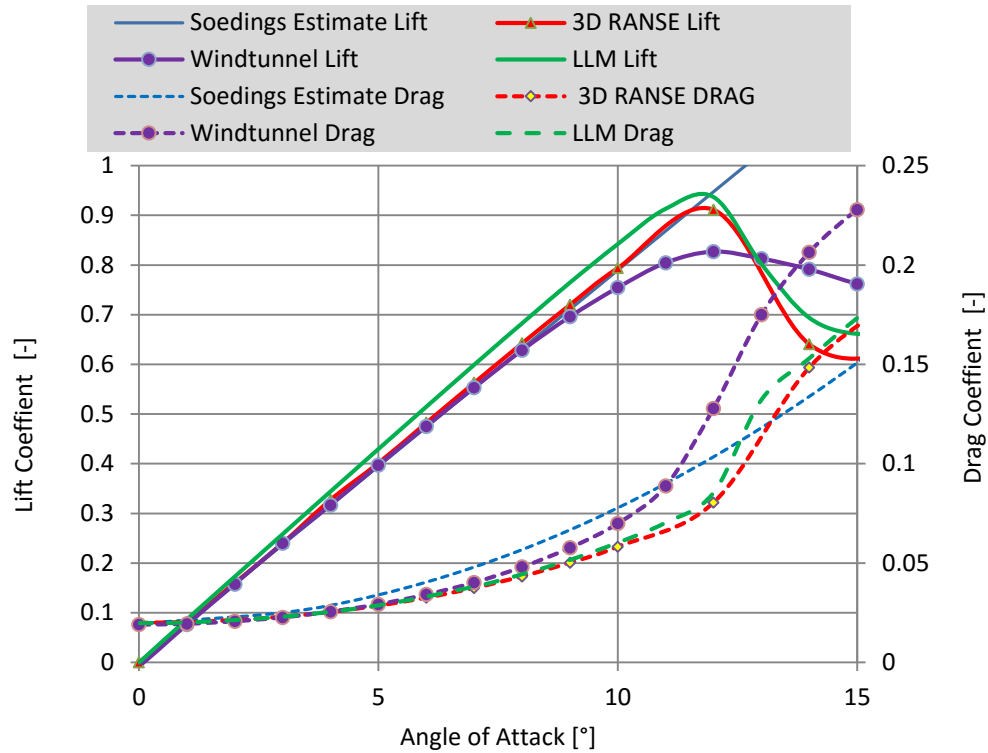


Figure 4-5: Comparison of 3D-RANS investigations with lifting line method and wind tunnel test results

## 4.2 AC72 TYPE TWO-ELEMENT WING

The second test case is a two-element wing designed in accordance with but not strictly following the rules for the AC72 catamaran (see Americas Cup Race Management (2012)). The wing has a span of 38 m and a planform area of 260 m<sup>2</sup>. Leech and luff is fixed within the bandwidth given by the AC 72 rules. Some simplifications are made for the profile in order to reduce the computational load for the 2D-RANS investigations: the profile of the main element is a NACA 0020 while the second element profile is a NACA 64<sub>2</sub>-010. The chord ratio of main and second element is 1 over the entire span. This simplification allows analyzing only a single profile geometry for the 2D-RANS simulations, if Reynolds number effects are neglected. At zero flap angle the gap between main and second element is 10mm. The center of rotation of the second element is located at 85% of the chord length of the main element. Some additional simplifications apply in order to reflect the vertical partitioning of the flap into four panels. The root of the entire wing is located 0.5 m above a flat plate

This wing design, see Figure 4-6, by far does not suggest being an optimized one. The sole reason for this design is a simplification, which allows restricting 2D-RANS investigations to a single shape, assuming that changes of flow forces due to moderate changes of Reynolds number can be neglected.

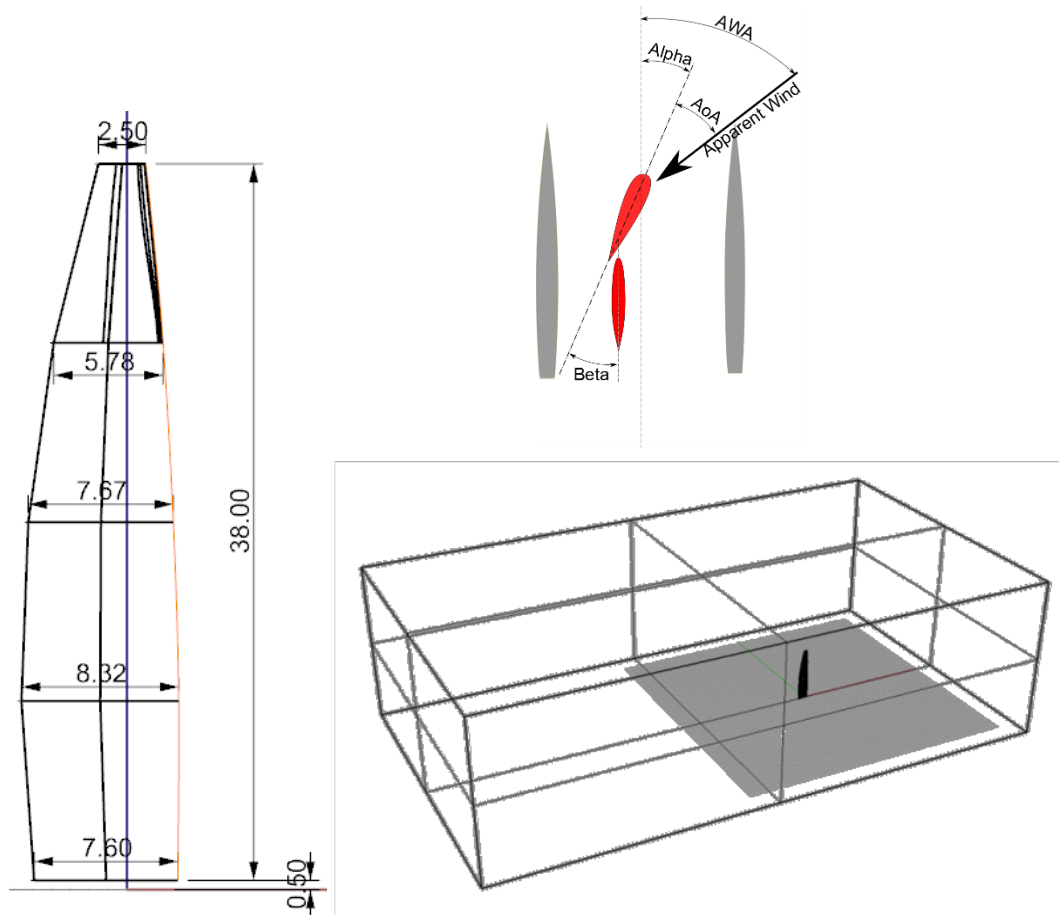


Figure 4-6: AC72 wing geometry and computational domain

### 4.3 COMPUTATIONAL GRID FOR 2D- AND 3D-RANS INVESTIGATIONS

Intensive grid sensitivity studies have been carried out in order to get grid-invariant simulation results. Grids of 5 million to 18 million grid cells have been investigated. The final 3D grid uses about 10.2 million Cartesian grid cells in the far field with cascading refinements in the vicinity of the grid and additional local refinements at leading and trailing edge and at the gap between main and second element, see Figure 4-7. Figure 4-8 shows the result of a grid invariance study. Here the lift and drag predicted for computational grid sizes of 5 million to 17 million grid cells are related to the results for the largest grid of 17 million grid cells. It is shown, that a grid of 10.2 million grid cells is a reasonable compromise between accuracy/grid independency of results versus computational costs. The 2D-grid has been even finer with about 380000 grid cells. For this grid the boundary layer has been fully resolved,  $y^+ \approx 1$ , see Figure 4-9.

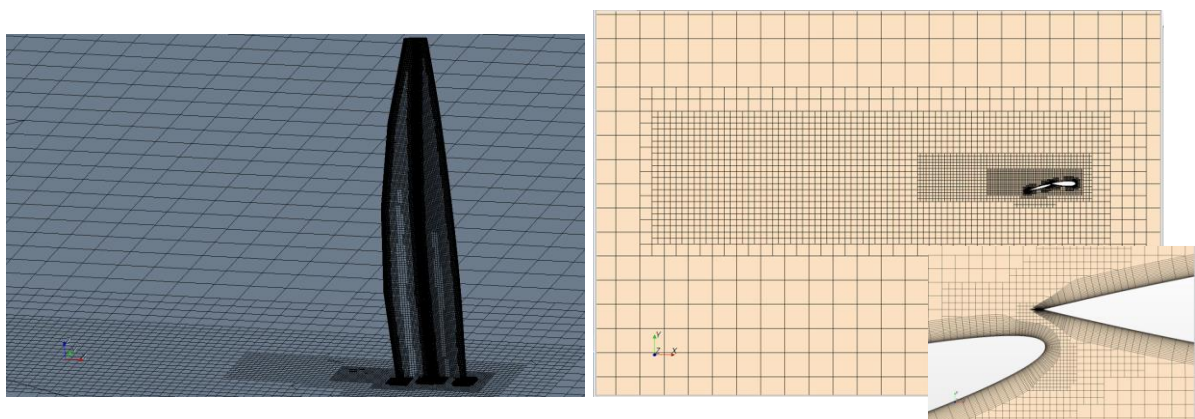


Figure 4-7: Computational grid of 3D RANS simulations around wing sail

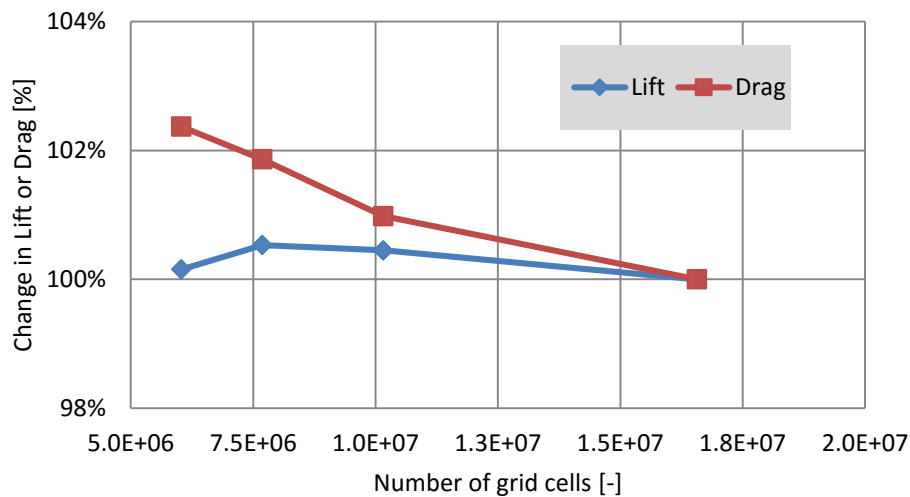


Figure 4-8: Result of grid sensitivity study

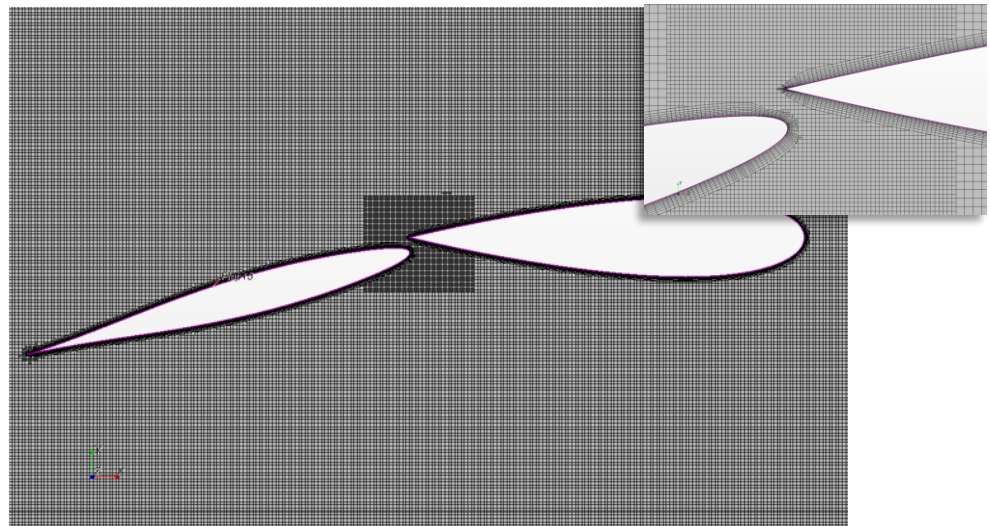


Figure 4-9: Computational grid for 2D RANS wing profile investigation

#### 4.4 2D-RANS SIMULATION RESULTS

2D RANS investigations have been carried out executing the following test matrix:

- 14 AoA with dense distribution of angles close to maximum lift
- 5 flap angles ranging from 0° to 20°

Some test calculations have been done using the SST turbulence model of Menter (1994). The unsteady RANS equations have been solved. Flow velocity has been set to a Reynolds number of about  $Re=5.0e6$  and turbulence intensity at inlet to 1%. The Reynolds number has been calculated from an average chord length (wing area / span) and a flow speed of 10 m/s.

Observations of the results however have shown conspicuous lift coefficients at higher angles of attack. In particular after reaching stalled conditions and the respective drop of lift coefficients the lift recovered and increased again with increasing angle of attack. This behavior cannot be found in experiments, suggesting the lack of the SST- and other 2-equation turbulence models to properly resolve stalled flow conditions.

As a remedy the entire range of AoAs and flap angles has been re-investigated using the Reynolds Stress Model of Gibson and Launder (1978). For 2D-flow this does not increase the number of unknowns and consequently the computational workload is the same as for a 2-equations turbulence model. The conspicuous behavior of lift at higher angle has been avoided at least to an acceptable degree. The 2D-RANS-results shown here use this Reynolds stress model.



Simulations have been conducted solving the unsteady RANS equation with 1<sup>st</sup> order time integration and a time step size of  $\Delta t=0.015$ s for 2D flow and  $\Delta t=0.15$  s for 3D-flow.

Figure 4-10 shows streamlines for angle of attack  $AoA=5^\circ$  and a contour plot of velocity magnitude for  $AoA=15^\circ$ . While the flow pattern looks as expected for low  $AoA$ , the unsteady vortex shedding at separated flow condition can clearly be depicted.

The unsteady vortex shedding obviously generated oscillating flow forces at stalled condition. For the calculation of lift and drag coefficients, some averaging over a larger number of time steps of the unsteady calculation has been employed. Typical simulation time is about 2 to 4 time the domain traveling time – the time, a flow particle needs to pass the entire domain. Only a small fraction of this is needed to reduce the average residuum of velocity by four orders of magnitude, the remaining time is used for flow force averaging, covering a large number of vortex shedding cycles.

Figure 4-11 and Figure 4-12 show lift coefficient over  $AoA$  and the drag over lift profile polar.

The second diagram shows an unexpected bump of the drag with increasing lift. The rational for this could not be completely unveiled within this study, however it can be assumed that this behavior can be linked to the flow mechanics in the gap between main element and flap.

A two-element-profile produces a particular amount of lift with a combination of main element angle of attack and flap angle, however there is usually just one combination of  $AoA$  and flap angle  $\beta$  for which the lift to drag ratio is a maximum. It can well be assumed that the very pronounced bump of the graph at flap angle of  $20^\circ$  is generated by a flow pattern where the gap has a positive impact on the boundary layer at the trailing edge of main element as well as the leading edge of the flap, preventing the boundary layer to separate there. This will result in a maximum lift to drag ratio.

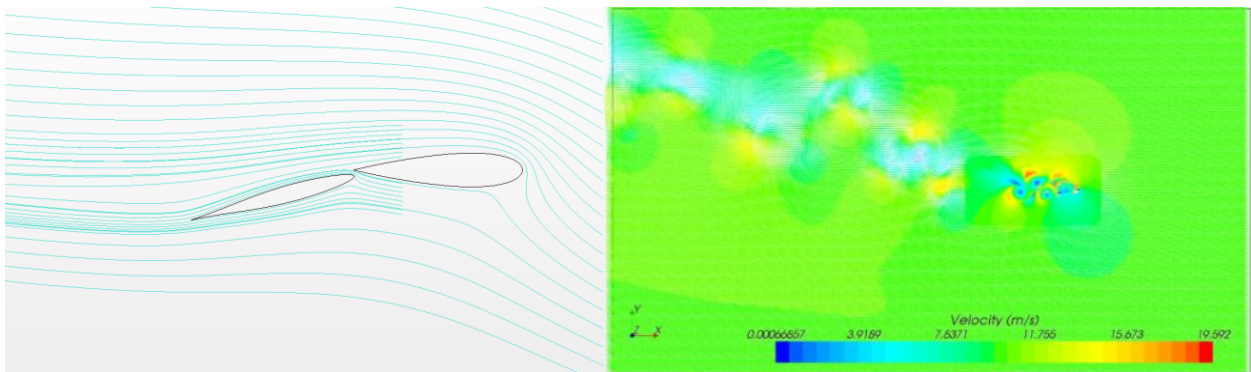


Figure 4-10: Streamlines at  $AoA=14^\circ$ , flap angle  $10^\circ$ , velocity magnitude contour plot at  $AoA=20^\circ$ , flap angle  $20^\circ$

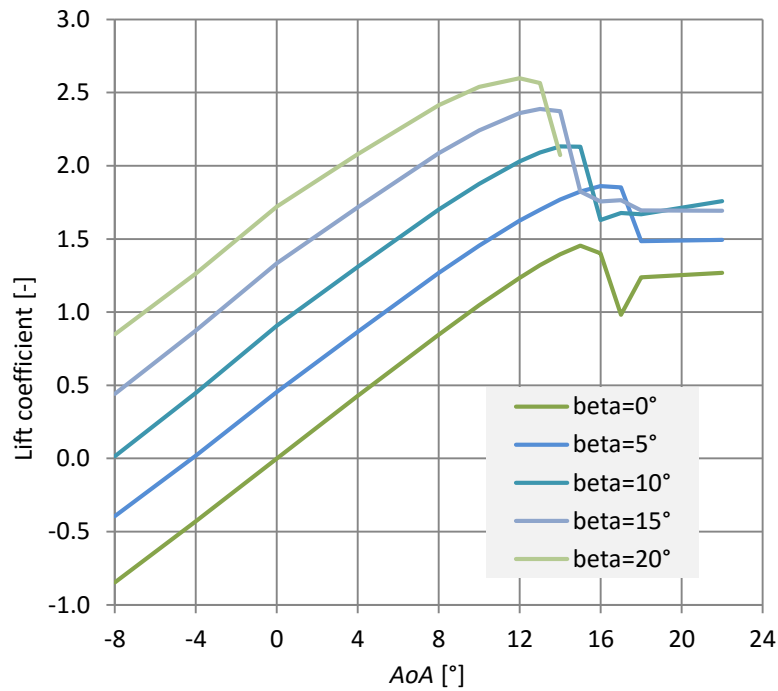


Figure 4-11: Lift coefficient over AoA for profiles at various flap angles beta

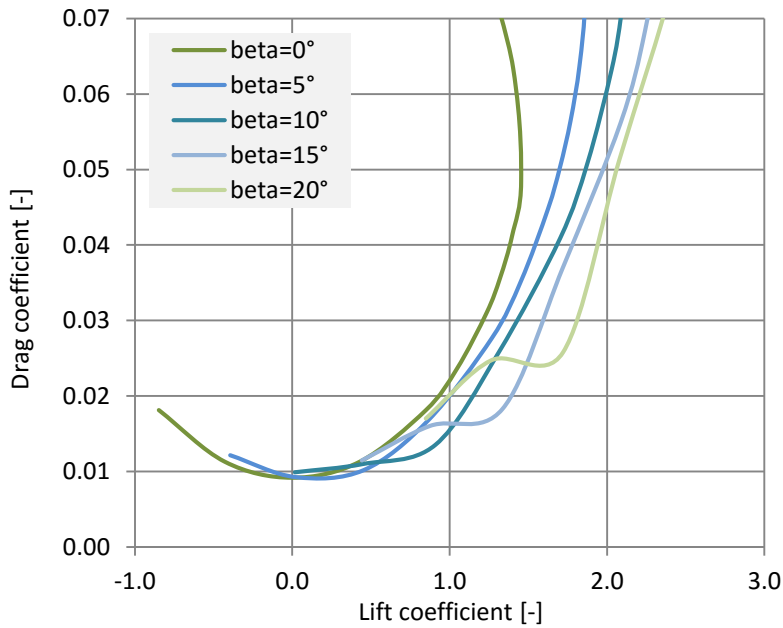


Figure 4-12: Drag over lift for profiles at various flap angles beta

#### 4.5 3D-RANS SIMULATION RESULTS AND COMPARISON WITH THE 2D-RANS – LIFTING LINE METHOD

Full 3D RANS investigation of the wing have been investigated for a test matrix of 13 angles of attack ranging from  $0^\circ < \text{AoA} < 22^\circ$ . These have been combined with flap angles of  $0^\circ < \beta < 20^\circ$ . A single twist case has been studied, where the flap angle at the root of the wing was  $\beta = 20^\circ$ , reducing linearly to  $\beta = 0^\circ$  at the tip.

Flow velocity was set to 10m/s. SST turbulence model has been used and turbulence intensity at inlet was set to 1%.

Figure 4-13 shows flow pattern at angle of attack of  $AoA=14^\circ$  and a flap angle of  $5^\circ$ . It shows beginning flow separation at the trailing edge of the main element.

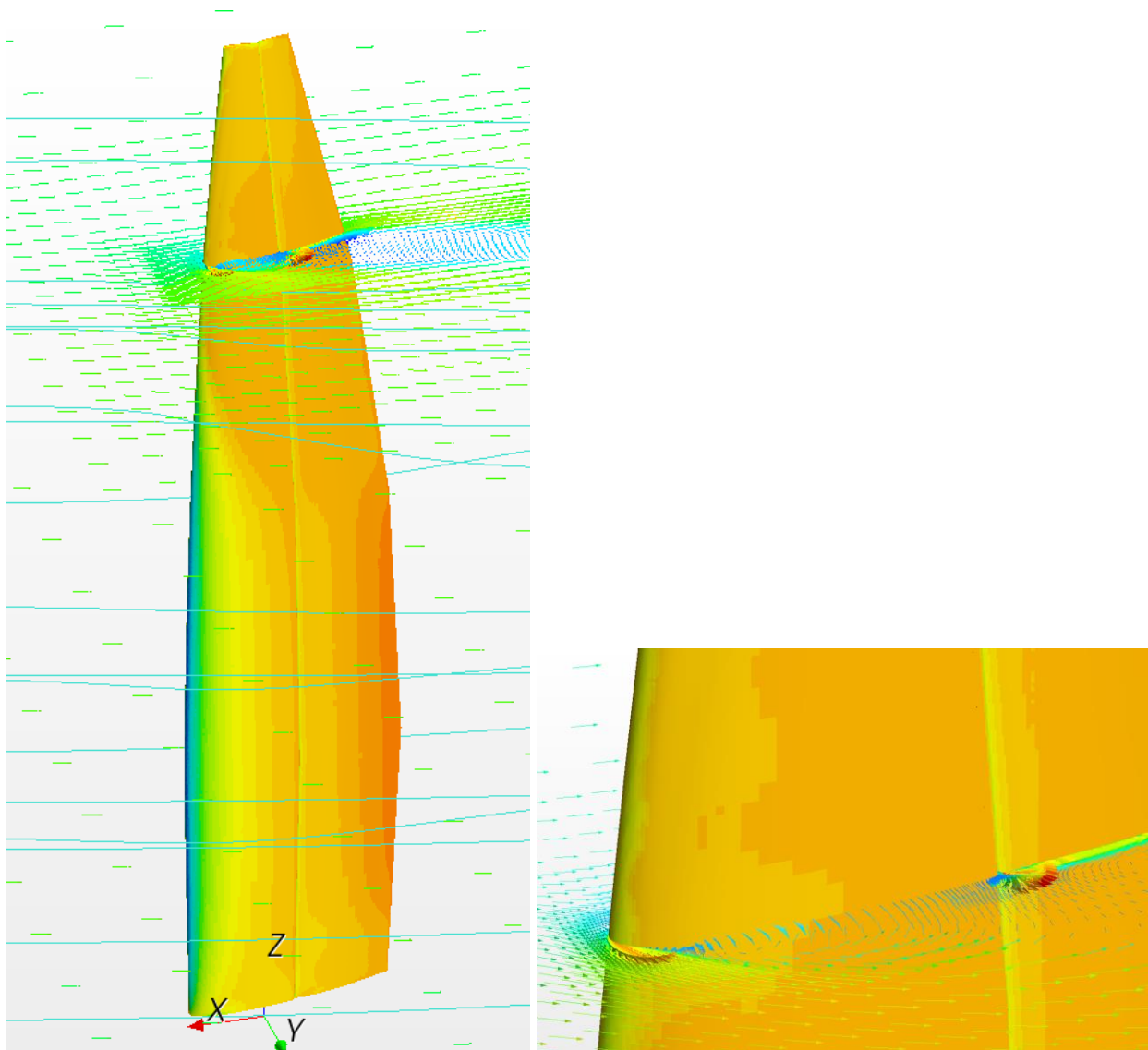


Figure 4-13: Flow pattern around wing

The 2D-RANS – Lifting line calculations are based on 21 horizontal profiles evenly distributed along span.

The distance of the wing from the catamaran platform is taken into account by the free vortex weighting factor. A value of  $\omega_{VF}=0.375$  has been estimated by an adjustment of the 2D-RANS-lifting line method results to the 3D-RANS-results for the flap angle of  $\beta = 10^\circ$  and  $AoA=10^\circ$ . It has been kept constant for the entire set of calculations shown here. Results of the 2D-RANS profile investigations have been integrated for the full range of the test matrix, including very large angles of attack with fully separated flow. Comparisons of the 3D-RANS results with those of lifting line method have been generated for the entire test matrix. However an excerpt of the results is shown here only.

Figure 4-14 to Figure 4-20 show lift and drag coefficients from 3D RANS simulations and the lifting line method over  $AoA$  for flap angles of  $0^\circ$ ,  $10^\circ$  and  $20^\circ$ , while Figure 4-17 and Figure 4-21 show lift and drag coefficients for the twisted test case.



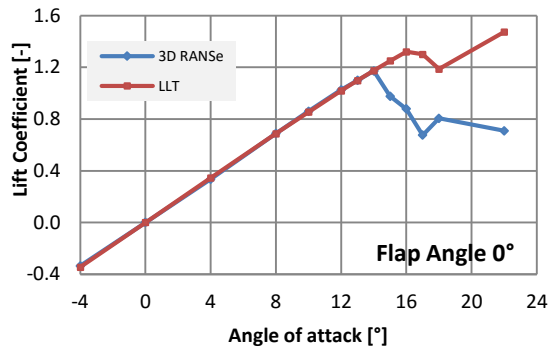


Figure 4-14: Lift coefficient over AoA, flap angle 0°

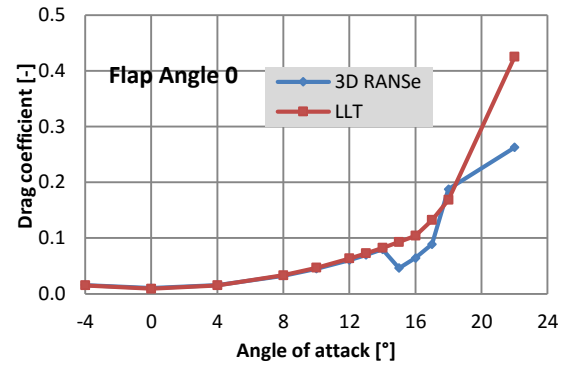


Figure 4-18: Drag coefficient over AoA, flap angle 0

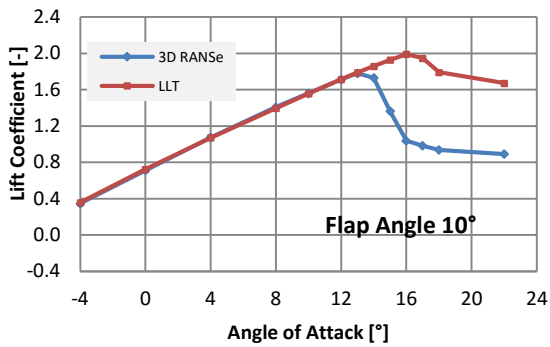


Figure 4-15: Lift coefficient over AoA, flap angle 10°

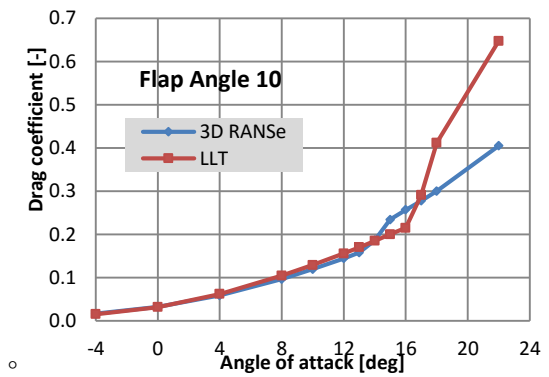


Figure 4-19: Drag coefficient over AoA, flap angle 10°

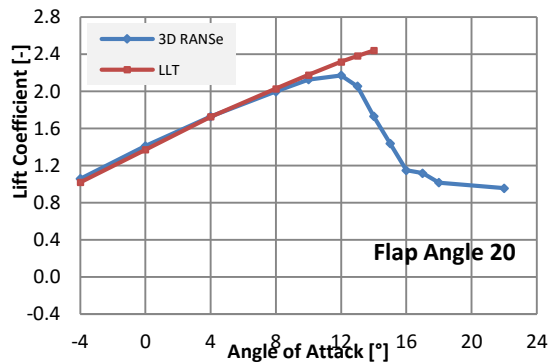


Figure 4-16: Lift coefficient over AoA, flap angle 20°

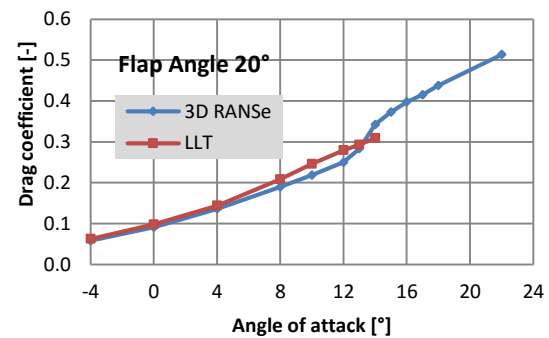


Figure 4-20: Drag coefficient over AoA, flap angle 20°

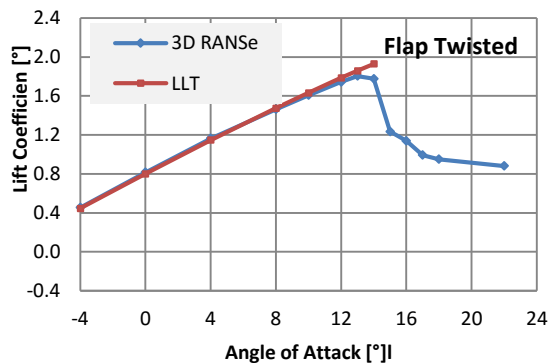


Figure 4-17: Lift coefficient over AoA, flap angle 0° (root) to 20° (tip)

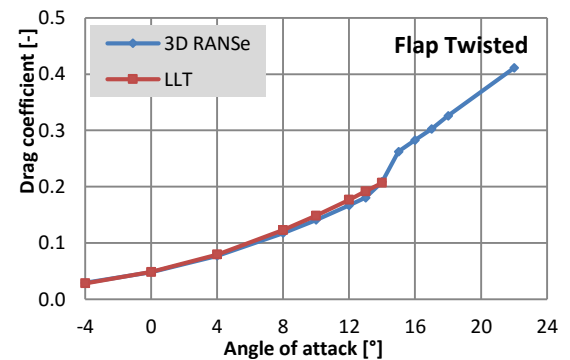


Figure 4-21: Drag coefficient over AoA, flap angle 0° (root) to 20° (tip)

## 4.6 ASSESSMENT OF THE RESULTS

A comparison of the 3D RANS results and those of the lifting line method shows a threefold trend:

- For small  $AoA$ s where no flow separation can be detected the agreement of the two methods is very good. This holds for the lift as well as the drag, which in case of the lifting line method is calculated as a sum of the induced drag from the LLT and the viscous drag from 2D RANS profile simulations
- For larger angles of attack and small flap angles the maximum lift coefficient is lower for the 3D RANS simulations. The  $AoA$  of maximum lift is predicted lower for the 3D RANS simulations. Beyond the  $AoA$  of maximum lift coefficient the lift from LLT is generally too large
- For very large flap angles the lifting line method is not able to predict a result. Here the nonlinearity of the 2D lift coefficient is so pronounced that the iterative method of the LLT fails to converge. It has been observed that the method generally started to diverge whenever some negative induced wind has been generated close to the tip of the wing, this due to large profile lift coefficients at the root.

It remains to be concluded that the 2D-RANS-lifting line method works well in the attached flow regime. It is capable to treat non-linear lift coefficients and can take flow separation into account. However for separated flow the results of the two methods compared show some deviation. It is assumed that this can be traced back to the three-dimensional nature of flow separation. Streamlines around and within a separated zone usually show a strong vertical component. This obviously cannot be modeled by the RANS solver profile investigations. In general it can be concluded that the method is well suitable for the investigation of wing sails at strong wind conditions. Due to hydrostatic stability constraints of the catamaran, at higher wind speeds the lift coefficients are rather small and flow separation can be avoided.

## 5 OPTIMIZATION OF TWIST AND ANGLE OF ATTACK

Once the lifting line method has been implemented and the results of the profile investigation properly integrated, the computational runtime to investigate a single wing is almost negligible. LLT calculations can be carried out on a standard PC and take no more than a few seconds to calculate lift and drag as well as side and driving forces and heeling moments for a particular planform and given settings for flow speed, angle of attack  $AoA$  and flap angle, which may vary with height in order to take into account wing twist. This opens the window for intensive optimizations studies of trim settings and planform within the preliminary design of a wing.

In the following examples the lifting line method has been combined with a constraint optimization method based on the Generalized Reduced Gradient method. This method is readily available within the Excel© spreadsheet calculation program. It is used to find trim settings of the wing for maximum driving force with a heeling moment constraint. Multihulls usually achieve maximum speed when the windward hull just starts flying and the righting moment achieves a maximum. In this particular case maximizing driving force is a good approximation for maximizing speed. This assumption neglects the impact of side-force generated induced resistance, however the assumption is reasonable. The side force can only be changed to a small degree for given heeling moment and due to the high speed the induced drag generally is only a small fraction of the total drag.

In the following example the wing angle with respect to centerline of the catamaran and the flap angle, the angle of the second elements centerline with respect to the main elements centerline, may change over span. They have been predicted for maximum driving force at a heeling moment constraint of  $M_{Xmax}=500kNm$ . The main element twist has been fixed to  $10^\circ$ , apparent wind angle to  $20^\circ$ .

For an apparent wind speed of  $AWS=12m/s$  the optimizer found the maximum of driving force of  $F_{Xmax}=7324$  N, at a wing angle of  $\alpha=9.3^\circ$ .

Figure 5-1 shows flap angle, lift and lift coefficient over span. It is assumed here that the flap angle may vary continuously. In reality the second element consists of 4 flaps, which are controlled independently. These flaps deflect under wind load, yielding an almost continuous variation of flap angle over span.

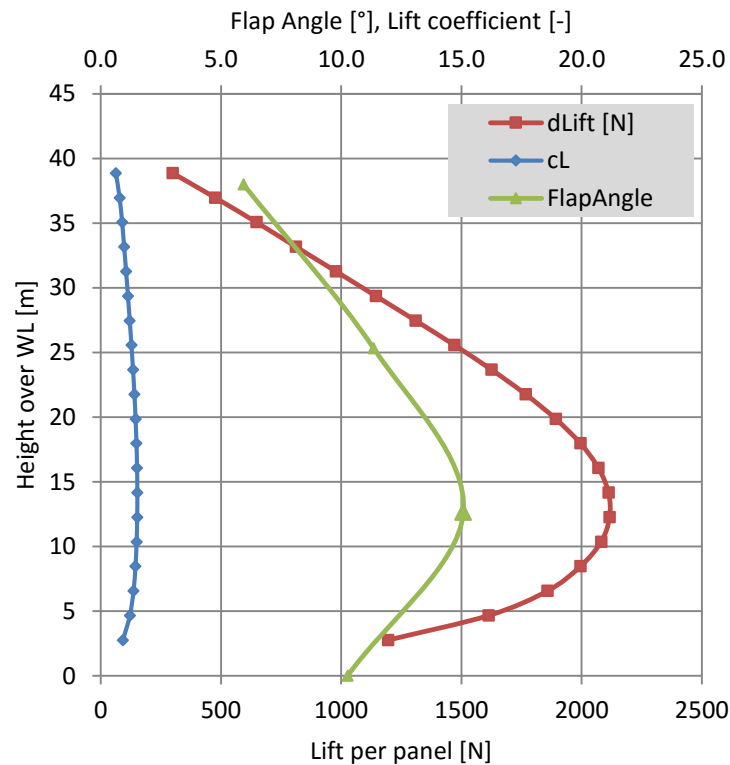


Figure 5-1: Lift, lift coefficient  $C_L$  and flap angle over span, AWS=12m/s

Figure 5-2 shows the results for the same calculation for AWS=18m/s. Here the result gives a driving force of  $F_{xmax}=9335$  N with a sheeting of the wing which is eased compared to the case of AWS=12m/s from  $\alpha=9.3^\circ$  to  $\alpha=13.8^\circ$ . The diagram clearly indicates that the optimizer not only eased the main element but also twists the flap significantly from an angle  $\beta=15^\circ$  at the base of the wing to a slightly negative value at the tip. The lift coefficient at the tip is slightly negative.

For an even higher apparent wind speed of AWS=24m/s this effect of twisting the flap is even more pronounced. Figure 5-3 shows lift, lift coefficient and flap angle over span for this case. Here the flap angle has been reduced dramatically and the top of the wing shows inverted twist, generating some righting moment. The driving force is  $F_{xmax}=11320$  N at a wing angle of  $\alpha=14.6^\circ$ .

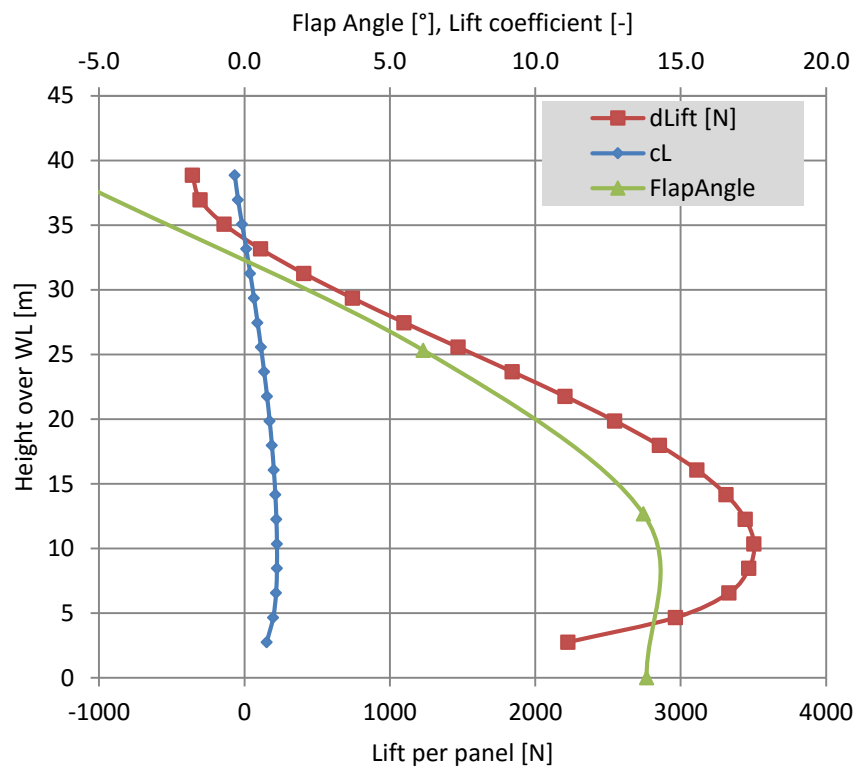


Figure 5-2: Lift,  $C_L$  and flap angle over span, AWS=18m/s

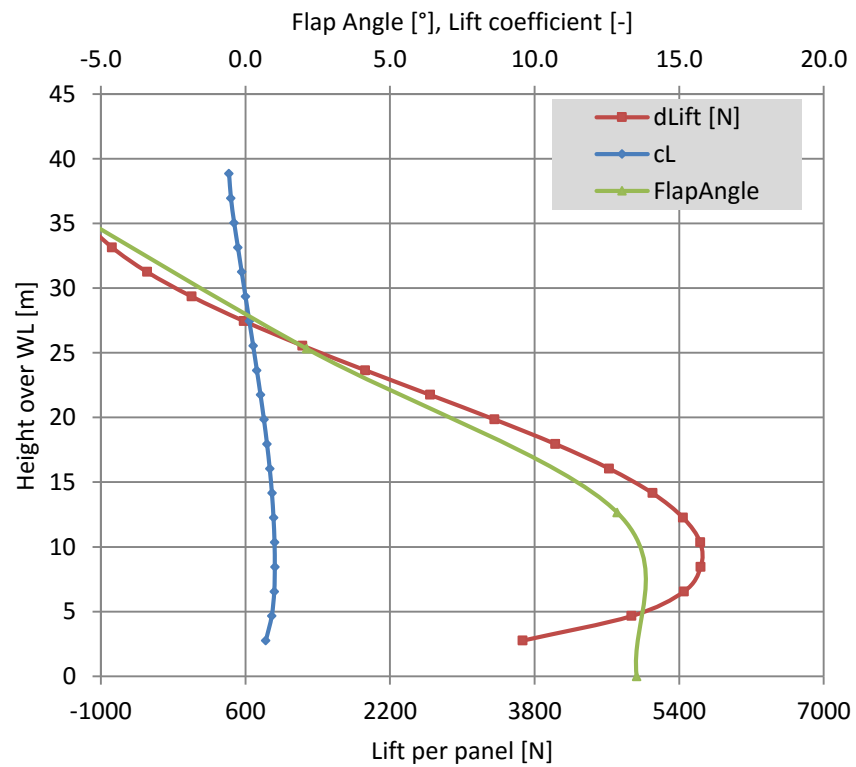


Figure 5-3: Lift,  $C_L$  and flap angle over span, AWS=24m/s

More results can be derived from the optimization calculations which may give hints for trimming the wing. The optimizer tries to minimize induced drag by maximizing effective span, however at higher wind speeds effective span is traded in against low vertical center of effort with respect to side forces.

Figure 5-4 depicts vertical center of effort  $VCE$  and effective span of the wing over apparent wind speed. Effective span has been calculated from:

$$s_{Eff} = \sqrt{\frac{L^2}{D_i 0.5 \rho AWS^2}} \quad (5-1)$$

The diagram shows that any reduction of  $VCE$  is costly with respect to induced drag.

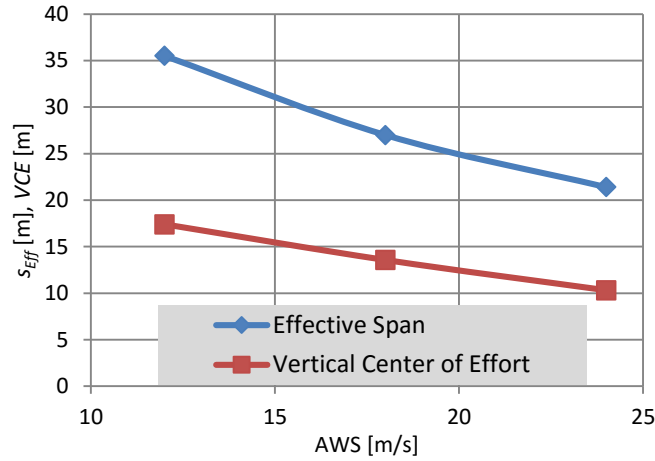


Figure 5-4: Effective span and VCE for optimum trim

As it has been mentioned earlier, the profile investigations are carried out at a constant Reynolds number of  $Rn=5.0e6$ , which yields from an average chord length and a flow speed of 10 m/s. The test cases investigated in this chapter use wind speeds of  $12\text{m/s} < AWS < 24\text{m/s}$ .  $AWS=24\text{ m/s}$  gives a Reynolds number 2.4 as high and consequently a friction drag coefficient reduction of 15%, compared to the case of  $AWS=10\text{ m/s}$ . The friction drag (the drag at zero lift) is only a small fraction of the total resistance. It thus can be assumed that the results obtained here are valid with reasonable accuracy, since the main free variable for the optimizations, angle of attack of main element and flap, influence the induced drag to a much higher extend than the friction drag.

## 6 CONCLUSIONS

The results from the two methods compared in the study presented here show a clear pattern: the lifting line method is well suitable to predict the performance of a two-element wing quite well in the attached flow regime. While the LLT method as implemented here principally can take flow separation into account, the flow force results generated in this regime diverge from those derived from 3D-RANS simulations.

While generally the confidence to provide accurate results is greater for a full 3D RANS simulation than for the combination of lifting line method with 2D-RANS simulations, it has to be understood that the simulation of separated flow is still error-prone for the turbulence models available for practical engineering investigations. Consequently it cannot be claimed that the 3D-RANS simulations based on the turbulence models employed in this study are sufficiently accurate on an absolute scale and agree fully with the reality. It is left to speculation only if the 3D-RANS results are closer to reality than the lifting line method results. Only a rigorous validation and verification study with qualified experimental results may enlighten this in more detail. This has been beyond the scope of the current study.

Where applicable, the lifting line method in combination with 2D-RANS simulation is of high value due to its computational efficiency. This holds obviously for the 2D-RANS simulations compared to those in 3D. In addition the principal of the employed lifting line method allows to be combined with constraint optimization methods. It can thus be used to find optimized trim settings of the wing for given wind conditions and hydrostatic constraints with very little effort. To do this based on 3D-RANS simulations; the computational load of such investigation easily can exceed any computational resources available to engineers. In addition 2D-RANS - lifting line method promises to be valuable for

the investigation of wing design alternatives, such as a planform study, which – once again – can be conducted with very little effort using conventional tools like a spreadsheet calculation program.

## **7 REFERENCES**

- Americas Cup Race Management, 2012. AC 72 Class Rules, [http://noticeboard.americascup.com/wp-content/uploads/2011/09/AC72\\_Class\\_Rule\\_v1-1\\_incl-Amendments-1-8.pdf](http://noticeboard.americascup.com/wp-content/uploads/2011/09/AC72_Class_Rule_v1-1_incl-Amendments-1-8.pdf).
- Anderson, J.D., c2011. Fundamentals of aerodynamics, 5th ed. McGraw-Hill, Singapore.
- Böhm, C., Graf, K., 2010. Validation of RANS simulations of a fully appended ACCV5 design using towing tank data, in: Royal Institution of Naval Architects (Ed.), Innovation in high performance sailing yachts (INNOV'SAIL 2010): International conference, 30 June - 1 July 2010, Lorient, France, RINA, London.
- Ferziger, J.H., Perić, M., 2008. Numerische Strömungsmechanik. Springer, Berlin, Heidelberg.
- Gibson, M.M., Launder, B.E., 1978. Ground Effects on Pressure Fluctuations in the Atmospheric Boundary Layer. *Journal of Fluid Mechanics* 86, 491–511.
- Harvald, S.A., 1983. Resistance and propulsion of ships. Wiley, New York.
- Menter, F.R., 1994. Two-equation eddy-viscosity turbulence models for engineering applications. *AIAA journal*.
- Söding, H., 1982. Prediction of Ship Steering Capabilities. *Ship Technology Research* 29, 3 ff.
- Truckenbrodt, E., Schlichting, H., 1967. Aerodynamik des Flugzeuges: Grundlagen aus der Strömungsmechanik Aerodynamik des Tragflügels Teil 1 und 2, 2nd ed. Springer, Berlin.